

Layer-by-layer assembly and UV-photoreduction of graphene-polyoxometalate composite films for electronics

Journal:	<i>Journal of the American Chemical Society</i>
Manuscript ID:	ja-2011-01594k.R2
Manuscript Type:	Article
Date Submitted by the Author:	06-May-2011
Complete List of Authors:	Li, Haolong; Max Planck Institute for Polymer Research, Materials Science Group Pang, Shuping; Max Planck Institute for Polymer Research Wu, Si; Max Planck Institute for Polymer Research Feng, Xinliang; Max-Planck Institute for Polymer Research, Synthetic Chemistry Mullen, Klaus; Max-Planck-Institute for Polymer Research; Max Planck Institute - Polymer Research Bubeck, Christoph; Max Planck Institute for Polymer Research, Materials Science

SCHOLARONE™
Manuscripts

1
2
3
4
5
6
7
8
9
10
11
12
13
14
15
16
17
18
19
20
21
22
23
24
25
26
27
28
29
30
31
32
33
34
35
36
37
38
39
40
41
42
43
44
45
46
47
48
49
50
51
52
53
54
55
56
57
58
59
60

Layer-by-layer assembly and UV-photoreduction of graphene-polyoxometalate composite films for electronics

Haolong Li,^{†,§} Shuping Pang,[†] Si Wu,[†] Xinliang Feng,^{,†} Klaus Müllen,^{*,†} and Christoph Bubeck^{*,†}*

[†]Max Planck Institute for Polymer Research, Ackermannweg 10, D-55128 Mainz, Germany

[§]State Key Laboratory of Supramolecular Structure and Materials, College of Chemistry, Jilin University, Changchun 130012, China

*Corresponding author. E-mail address: feng@mpip-mainz.mpg.de; muellen@mpip-mainz.mpg.de; bubeck@mpip-mainz.mpg.de

RECEIVED DATE (to be automatically inserted after your manuscript is accepted if required according to the journal that you are submitting your paper to)

Abstract Graphene oxide (GO) nanosheets and polyoxometalate clusters, H₃PW₁₂O₄₀ (PW), were co-assembled into multilayer films via electrostatic layer-by-layer assembly. Under UV irradiation, a photoreduction reaction took place in the films which converted GO to reduced GO (rGO) due to the photocatalytic activity of PW clusters. By this means, uniform and large-area composite films based on rGO were fabricated with precisely controlled thickness on various substrates such as quartz, silicon, and plastic supports. We further fabricated field effect transistors based on the composite films, which exhibited typical ambipolar features and good transport properties for both holes and electrons. The on/off ratios and the charge carrier mobilities of the transistors depend on the number of deposited layers

1 and can be controlled easily. Furthermore, we used photomasks to produce conductive patterns of rGO
2 domains on the films, which served as efficient microelectrodes for photodetector devices.
3
4

5 **Introduction**

6
7
8 Graphene has inspired great enthusiasm owing to its extraordinary properties including high charge-
9 carrier mobility and optical transparency, as well as flexibility, robustness and environmental stability.¹⁻⁴
10 It is a promising candidate for a plethora of electronic applications, particularly for thin film electronic
11 devices.⁵⁻⁷ Recently, graphene oxide (GO) has emerged as a suitable precursor for large-scale production
12 of graphene materials due to its cost-effective synthesis and superior solution processability.^{8,9}
13 Furthermore, oxygen containing groups on insulating GO nanosheets can be removed by reduction,
14 forming reduced graphene oxide (rGO) with improved electronic properties,¹⁰ which opens an effective
15 route to graphene materials for electronic applications.¹¹ However, to realize practical rGO-based
16 electronic devices, a precondition is to fabricate high quality rGO films with large-area uniformity. So
17 far, several methods have been developed to prepare rGO films, such as drop casting,¹² dip coating,¹³
18 spin coating,¹⁴ and vacuum filtration.^{15,16} Although these methods succeeded in fabricating some rGO
19 film devices, they suffer from distinct drawbacks: methods such as drop casting, dip coating, and spin
20 coating methods have difficulties in preparing uniform rGO films with the thickness of several
21 nanometers and vacuum filtration still need a film transfer procedure. Therefore, it is a challenging task
22 to develop a suitable method to overcome the obstacles described above.
23
24
25
26
27
28
29
30
31
32
33
34
35
36
37
38
39
40
41
42

43 Layer-by-layer (LBL) assembly is a widely used method for thin film fabrication and has been
44 applied to produce multilayer films of charged organic polymers, nanoparticles, and other inorganic
45 materials.¹⁷⁻¹⁹ The LBL method is based on the alternating adsorption of oppositely charged species
46 from dilute solutions onto substrates. It is simple, effective, and has the advantage of preparing films
47 with controlled nanometer thickness and uniformity over large areas. It has been reported that GO
48 nanosheets can adsorb on polyelectrolytes to form LBL assembled multilayers,^{20,21} owing to their
49 negatively charged surface in aqueous solution.¹⁶ Therefore, it is reasonable to believe that LBL
50 assembly can offer a promising means to fabricate high quality GO thin films.
51
52
53
54
55
56
57
58
59
60

1 When uniform GO thin films are available, the next important step is to convert GO to rGO by
2 suitable reduction methods which re-establish the special electronic properties of graphene. Currently,
3 GO reduction methods mostly rely on chemical and thermal reduction. However, toxic agents such as
4 hydrazine are often used in chemical reduction processes, and the high temperature treatment of thermal
5 reduction is not suitable for plastic electronics. For comparison, photoreduction, as a mild and
6 environment friendly method, is now receiving attention as an alternative approach for producing
7 rGO.²²⁻²⁶ Furthermore, photoreduction can be easily triggered by light, allowing to pattern circuit-like
8 structures such as in well-established photolithography, which is very appealing for microelectronic
9 industries.²⁴ We have reported that a Keggin-type polyoxometalate cluster, $H_3PW_{12}O_{40}$ (PW), can act as
10 an effective photocatalyst to reduce GO nanosheets in water solution under UV-irradiation, yielding
11 rGO with good electrical conductivity.²⁶ In principle, this type of photoreduction process can also be
12 performed in thin films consisting of GO nanosheets and PW clusters. On the other hand, the anionic
13 surface of polyoxometalate clusters allows to incorporate them into polyelectrolyte films by electrostatic
14 attraction.²⁷⁻³¹ Therefore, we envision that GO and PW can be co-assembled into multilayer films via
15 LBL alternating deposition.

16
17
18
19
20
21
22
23
24
25
26
27
28
29
30
31
32
33
34
35 In this work, we demonstrate the fabrication of high quality rGO composite films by means of the
36 LBL assembly procedure. GO nanosheets and PW clusters were incorporated in multilayer films, and a
37 subsequent in-situ photoreduction procedure converted GO to rGO due to the photocatalytic activity of
38 PW. In this way, ultrathin and large-area rGO films were easily and reproducibly prepared with several
39 nanometers thickness and uniform morphology. Thin film field effect transistors (FET) based on these
40 graphene films were fabricated, showing typical ambipolar characteristics and good transport properties
41 for both electrons and holes. The on/off ratios and the mobilities of the transistors can be easily tailored
42 by varying film thickness and thus the number of deposited layers. Furthermore, we used photomasks to
43 produce conductive patterns of rGO domains with the size down to several micrometers, which were
44 directly generated on the initial GO-PW composite films. Importantly, the rGO patterns can serve as
45 microelectrodes, e.g. for photodetector devices.

Results and discussion

Layer-by-layer assembly of GO-PW films. GO was oxidized from natural graphite flakes by a modified Hummers method.³² The pH value of GO solution is ~ 7 and its zeta potential is about -40 mV, which means that GO nanosheets are negatively charged.¹⁶ GO and PW both show characteristic absorptions in the UV-Vis region, as presented in Figure 1A. Two absorption bands of GO appear at 230 and 300 nm respectively, while the well-known ligand-to-metal charge transfer (LMCT) transition band of PW is located at 260 nm with an extinction coefficient of $\sim 7.5 \times 10^4 \text{ M}^{-1}\text{cm}^{-1}$. Therefore, it is easy to monitor the formation of GO-PW multilayer films by UV-Vis spectroscopy, according to the film absorbance at the characteristic absorption bands of GO and PW.

In the LBL assembly process, electrostatic interaction is the driving force owing to the negative charged surface of GO nanosheets and PW clusters in water solution. Firstly, the substrates were modified by a PEI/PW double layer as precursor films, and then different numbers of PAH/GO/PAH/PW layers were deposited on the modified substrates to construct GO-PW multilayer films, in which GO nanosheets and PW clusters are linked by PAH layers. In such a film structure, the PW layers exist on both sides of the GO layers. This design aims to realize an effective interaction between oxygen-containing groups on GO nanosheets and PW clusters, which is favorable for the electron transfer from photo-excited PW to GO, thus realizing an efficient reduction of GO in the subsequent PW-assisted photoreduction process. Figure 1B displays the UV-Vis absorption spectra of $(\text{PAH/GO/PAH/PW})_n$ multilayer films (with $n = 1-6$) assembled on a PEI/PW precursor film on quartz substrates. The absorption of the films increases systematically with the layer number n , which is evidence for the subsequent deposition of GO and PW components. When monitoring the detailed absorption variation during a PAH/GO/PAH/PW assembly process, the absorbance of films is found to increase after each deposition processes of GO and PW, implying that the two components are indeed assembled into the films (see Figure S1 in the supporting information). PAH does not absorb above 200 nm. Therefore, its presence in the films is not reflected in the absorption spectra. The absorbance values

1 for (PAH/GO/PAH/PW)_n multilayer films with n = 1-6 at 230, 260, and 300 nm are plotted as function
2
3
4 of the layer number n, as shown in the inset of Figure 1B. Apparently, the absorbance varies linearly
5
6 with n at all three wavelengths, which reveals a constant increase in the total amount of GO and PW
7
8 adsorbed in the films after each deposition cycle of PAH/GO/PAH/PW layer. Furthermore, the film
9
10 fabrication is highly reproducible. It is noted that the absorption variation of four separately prepared
11
12 (PAH/GO/PAH/PW)₆ films shows the consistent linear relationship with layer numbers, and the fitted
13
14 plots overlap well, as revealed in Figure S2, S3, and S4 in the supporting information. Such a
15
16 reproducible production guarantees the advantage of the LBL assembly method in precisely controlling
17
18 the film structure and thickness, which fulfills the requirement for electronic applications.
19
20
21

22
23 Based on the UV-vis spectra it is possible to calculate the surface coverage density Γ of PW clusters
24
25 in each PAH/GO/PAH/PW layer, by using the relation $\Gamma = (N_A A_\lambda) / 2 \varepsilon_\lambda$, where N_A is Avogadro's constant
26
27 ($6.02 \times 10^{23} \text{ mol}^{-1}$), A_λ is the absorbance of PW in a PAH/GO/PAH/PW layer at a given wavelength λ ,
28
29 and ε_λ is the isotropic molar extinction coefficient of PW at λ .^{27,34} In the current calculation, the relative
30
31 maximum λ_{max} of the LMCT transition band of PW at 260 nm is used. From Figure S1 in the supporting
32
33 information, we can obtain the A_{260} value (~ 0.01) from the variation of film absorbance resulting from
34
35 the adsorption of one layer PW in PAH/GO/PAH/PW film. This value is divided by 2 to give a surface
36
37 density for a single layer of PW, since the films were deposited on both sides of quartz substrate. ε_{260} of
38
39 PW is $\sim 7.5 \times 10^4 \text{ M}^{-1} \text{ cm}^{-1}$ as mentioned above. By using the above parameters, the average PW surface
40
41 coverage density of 4×10^{13} clusters per cm^2 is obtained, which corresponds to an average area per PW
42
43 of 2.5 nm^2 . Assuming that a single PW cluster has an area of approximately 0.8 nm^2 due to its T_d -
44
45 symmetric spherical shape and 1 nm diameter,³⁵ the average surface coverage of PW is calculated to be
46
47 $\sim 32\%$. It has been reported that a high ionic strength condition can screen the electrostatic repulsive
48
49 interaction between small polyoxometalate clusters (1 to 2 nm in diameter), enabling the clusters come
50
51 into close contact, which eventually gives rise to multilayer coverage.³¹ In principle, multilayer coverage
52
53 will induce a larger surface roughness which is unfavorable for the electronic device fabrication.
54
55
56
57
58
59
60

1 Therefore, we carried out the electrostatic deposition of PW in its pure aqueous solution without
2 additional salts, which is a typical low ionic strength condition and effectively avoids the formation of
3 multilayer coverage.
4
5

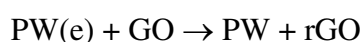
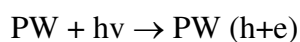
6
7 The surface morphology of the GO-PW films was characterized by atomic force microscopy (AFM)
8 measurement. The AFM image of a (PAH/GO/PAH/PW)₁ film on silicon substrate is shown in Figure
9 2A. Obviously, the film is covered by a monolayer of GO nanosheets with a high surface coverage,
10 although some nanosheets overlap at the edge regions. The root-mean-square deviation value of the
11 surface roughness (R_q) for the whole region in Figure 2A ($10 \times 10 \mu\text{m}^2$) is 1.17 nm, indicating a very
12 smooth surface of the film. Furthermore, the smooth surface morphology is uniformly distributed over
13 the whole region of a large-area film ($1 \text{ cm} \times 2 \text{ cm}$), by comparing the AFM images of different
14 positions on the film. Such a uniform morphology is an intrinsic advantage of LBL-assembly method,
15 which further determines the excellent electronic property of the films as discussed below. The
16 magnified AFM image of a (PAH/GO/PAH/PW)₁ film (Figure 2B) shows that small PW domains exist
17 uniformly on the surface of GO nanosheets, which are several square nanometers large and appear 2 to 3
18 nm higher than their surroundings. The domains are ascribed to the PW clusters adsorbed on PAH
19 chains.³¹ The uniform adsorption of PW clusters endows the (PAH/GO/PAH/PW)₁ film a very smooth
20 surface morphology, as the R_q value of the $1 \times 1 \mu\text{m}^2$ area in Figure 2B is only 0.59 nm. On the other
21 hand, the AFM images of (PAH/GO/PAH/PW)₆ films show a tight stacking morphology of multilayer
22 GO nanosheets (Figure 2C). Meanwhile, the area of PW domains increased to more than ten square
23 nanometers and the film roughness also become larger slightly (see Figure 2D). Increased roughness is
24 commonly observed for the first few layers in LBL assembled multilayer films, due to a substrate
25 effect.³¹ Even though, the roughness measurement of (PAH/GO/PAH/PW)₆ films still shows a rather
26 smooth surface: the R_q values of the $10 \times 10 \mu\text{m}^2$ area in Figure 2C and the $1 \times 1 \mu\text{m}^2$ area in Figure 2D
27 are 2.46 nm and 0.90 nm, respectively, which are only two times larger than the (PAH/GO/PAH/PW)₁
28 film. A large-area SEM image of (PAH/GO/PAH/PW)₆ films further confirms its smooth surface (see
29 Figure S5 in the supporting information). The low roughness between 1 to 2 nm of the GO-PW
30
31
32
33
34
35
36
37
38
39
40
41
42
43
44
45
46
47
48
49
50
51
52
53
54
55
56
57
58
59
60

1 multilayer films is certainly advantageous for the fabrication of large-area thin-film electronic devices.
2
3 According to the height profile, the thickness of (PAH/GO/PAH/PW)₆ film is approximately 12 nm (see
4
5 Figure S6 in the supporting information). By subtracting the thickness of (PAH/GO/PAH/PW)₁ film
6
7 from that of (PAH/GO/PAH/PW)₆ film and dividing the result by 5, the average effective thickness per
8
9 PAH/GO/PAH/PW is estimated to be 2 nm. This value is smaller than the total thickness of 3.9 nm
10
11 expected for an ideal multilayer by using literature data: one layer of PW cluster (1 nm),³⁵ one layer of
12
13 GO nanosheet (0.9 nm),²⁶ and two layers of PAH (2 nm).³⁰ We attribute the difference to an inadequate
14
15 occupancy of PW clusters in each layer, because its surface coverage density is only 32 % as discussed
16
17 above.
18
19

20
21 **UV-photoreduction of GO-PW films.** GO-PW multilayer films were prepared on different
22
23 hydrophilic substrates, such as quartz and oxygen plasma treated flexible PET substrates,³³ by means of
24
25 the LBL-assembly method described above, as shown in Figure 3A and 3C. However, these GO-PW
26
27 films are insulating due to the nature of the GO nanosheets.⁸⁻¹¹ An in-situ photoreduction of the films
28
29 was employed to convert the GO nanosheets into conductive rGO. In the photoreduction procedure, the
30
31 GO-PW multilayer films were irradiated by a 100 W high pressure mercury lamp (combined with filters
32
33 to provide $\lambda > 280$ nm) to oxidize the organic polyelectrolytes and reduce the GO nanosheets by using
34
35 the photocatalytic activity of PW clusters.²⁶ The color of the films gradually turned from light brown to
36
37 dark (Figure 3B and 3D), suggesting the successful formation of rGO.
38
39
40
41

42
43 Figure 4A shows the UV-Vis spectra of the films in the whole UV-Vis region. The absorbance of the
44
45 films gradually increases with the irradiation time of UV light, and its value rises up to a plateau after
46
47 about 6 hours, which means that the photoreduction reaches a saturation state (inset of Figure 4A). AFM
48
49 characterization indicates that the reduced GO-PW films possess the same surface morphology as the
50
51 original film, suggesting the mild photoreduction conditions of the present method. A detailed
52
53 comparison of the film morphologies before and after photoreduction will be presented below. In
54
55 contrast to our observation, Huang et al. reported that the photoreduction can be dominated by a
56
57 photothermal heating effect, which causes significant expansion of the thickness of GO films, about 10
58
59
60

1 times to the original films, and thus the film morphology was unavoidably changed.²⁴ However, in our
2 work, the temperature of samples was kept at room temperature due to the weak heating effect of UV
3 light and the use of an airflow cooling system. Therefore, the photoreduction process should be
4 determined by a photochemical reaction, with the same mechanism as was presented for the PW-assisted
5 photoreduction in solution.²⁶ The photocatalytic activity of PW is similar to semiconductor
6 nanoparticles, such as TiO₂ nanoparticles. Under the irradiation of UV light, the O → W charge transfer
7 band in PW cluster is excited, which leads to electron hole separation.³⁶ The excited PW clusters can
8 play the role of both oxidant and reductant. It has been reported that photo-excited titania nanosheets can
9 oxidize PAH in LBL films,²⁵ from which a similar process can be concluded in the present GO-PW
10 composite films: PAH is oxidized by excited PW. On the other hand, the electrons trapped in the cage-
11 type structure of excited PW clusters transfer to GO nanosheets, resulting in the reduction of GO. In the
12 whole photoreduction process, PW acts as photocatalyst and electron relay.^{36,37} This process can be
13 described as:
14
15
16
17
18
19
20
21
22
23
24
25
26
27
28
29



33 Similar mechanisms have also been proposed earlier in the systems of GO and other semiconductor
34 nanoparticles such as TiO₂ and ZnO.^{22,23} It is worth noting that the photoreduction was efficient even in
35 air atmosphere, because the oxygen in air can oxidize the photo-excited PW to ground state and lower
36 the photocatalytic effect.³⁶ Here, we believe that the tight interaction of GO layer, PW layer, and PAH
37 layer in LBL films can prevent PW clusters from exposing to external oxygen, thus leading to an
38 efficient photoreduction process. It should be noted that the photoreduction can not take place without
39 PW in the films. In our previous work using PW to photoreduce GO in water solution, we also found
40 that the photoreduction did not occur if PW was not added into the solution.²⁶ Therefore, the
41 photocatalytic activity of PW is crucial for GO reduction in the present work.
42
43
44
45
46
47
48
49
50
51
52
53
54
55
56
57
58
59
60

1 X-ray photoelectron spectroscopy (XPS) was employed to analyze the compositional change of
2 carbon atoms in different chemical states of GO-PW films before and after photoreduction. Figure 4B
3 shows the C 1s XPS spectra before and after UV-irradiation. Four types of carbon with different
4 chemical states are observed, which appear at 284.5 eV (graphite, C–C/C=C), 286.6 eV (C–O), 287.8
5 eV (C=O), and 289.0 eV (O–C=O), respectively. Both XPS spectra were fitted to evaluate the relative
6 areas of the peaks. The results are shown in Table 1. Inspection of Figure 4B and Table 1 shows that the
7 relative areas of all peaks corresponding to oxygen containing groups decreased when the film
8 underwent a 6 hour photoreduction. In particular, the percentage of the C-O group greatly decreased
9 from initial 41.1 % to 20.9 %, which suggests that many oxygen containing moieties have been
10 eliminated by photoreduction. Meanwhile, the content of C–C/C=C group increased from to 44.8 % to
11 65.6 %, indicating that significant sp^3/sp^2 hybridized carbon structures were restored.

12 The electrical conductivity measurement of rGO also provides a means to judge the reduction degree
13 of GO. After 6 hour photoreduction, photoreduced rGO-PW films of (PAH/GO/PAH/PW)₁ and
14 (PAH/GO/PAH/PW)₆ show a conductivity of about 10 S m⁻¹ and 120 S m⁻¹, respectively. Apparently,
15 these values are comparable to those of the rGO films produced by chemical methods,³⁸ highlighting the
16 efficient conversion of GO to rGO in this work.

17 **Electronic properties of rGO-PW films.** Electronic applications represent one of the most
18 important research fields of rGO-based materials.⁹⁻¹¹ For this, the fabrication of rGO-based transistors
19 has attracted particular attention, which requires the preparation of high quality and ultrathin rGO films
20 with uniform morphology on large-area substrates.¹¹ The rGO-PW composite films fulfill these
21 necessities. To demonstrate the transport performance of these graphene films, we fabricated FET
22 devices based on (PAH/GO/PAH/PW)₁ films and (PAH/GO/PAH/PW)₆ films, respectively. Scheme and
23 optical images of typical FET devices are depicted in Figures 5A and 5B. Both films were deposited on
24 silicon substrates, which had a 300 nm thermal oxide layer. Au electrodes with a channel width of 400
25 μm and a channel length of 20 μm were thermally evaporated on the films as source and drain
26 electrodes. The silicon substrate was used as gate electrode and the thermal oxide layer on the silicon
27

1 surface acted as insulator layer. The FET devices both exhibit ambipolar field effect, which is typical for
2 graphene transistors,¹⁵ see Figure 5C and 5D. Electron and hole mobilities can be extracted from the
3 linear regime of the transfer characteristics, using the equation $\mu = [(\Delta I_{sd}/\Delta V_g) * (L/W)] / C_{ox} V_{sd}$,⁶ where L
4 and W are channel length and width, C_{ox} is the capacitance of silicon oxide gate (which is 1.27×10^{-8}
5 F/cm² for a 300 nm thick silicon oxide), V_{sd} is the source-drain voltage which is 10 V in the present
6 work, I_{sd} is the source-drain current, and V_g is the gate voltage. $\Delta I_{sd}/\Delta V_g$ is the transconductance or the
7 slope of the transfer curve in the linear regime. From the I_{sd} - V_g curves, we can derive the hole and
8 electron mobility values of $\mu_h = 0.03$ and $\mu_e = 0.01$ cm²V⁻¹S⁻¹ for the (PAH/GO/PAH/PW)₁ film device,
9 and $\mu_h = 0.15$ and $\mu_e = 0.06$ cm²V⁻¹S⁻¹ for the (PAH/GO/PAH/PW)₆ film device, respectively. It has
10 been reported that adsorbing small molecules such as water and oxygen on rGO FET devices results in
11 hole-dominated transporting.^{39,40} In our work, the cage-type structure of PW can trap electrons,³⁶ which
12 probably causes that the rGO-PW FET devices exhibit a hole-dominated transport behavior. The on/off
13 ratio, which is defined as the ratio of maximum value and minimum value of I_{sd} , of the
14 (PAH/GO/PAH/PW)₁ film device is ~ 2.0 and that of the (PAH/GO/PAH/PW)₆ is ~ 1.1. These values
15 are similar to those reported for rGO films prepared by chemical or thermal reduction methods.^{15, 39-41}
16 Thereby, it is evident that the electronic transport properties of the as-fabricated FET devices greatly
17 depend on the film thickness: The devices with thicker films exhibit a higher mobility and a lower
18 on/off ratio. As discussed above, the thickness of rGO-PW film can be precisely adjusted by controlling
19 the number of deposited layers. This feature makes our method well superior for the fabrication of rGO-
20 based FET devices with tailorable properties. Furthermore, we note that all the FET devices distributed
21 on a 1 cm × 2 cm large-area film work well and exhibit similar transport properties, which we attribute
22 to the high uniformity of the films.

23
24
25
26
27
28
29
30
31
32
33
34
35
36
37
38
39
40
41
42
43
44
45
46
47
48
49
50
51
52
53
54
55
56
57
58
59
60

Besides their use as active components in transistors, graphene films have another important application as electrode material.¹¹ Although several methods for film preparation, such as spin coating, dip coating, and vacuum filtration involving a chemical or thermal reduction procedure, have been developed to fabricate rGO-based electrodes, the direct fabrication of patterned thin-film electrodes still

1 remains difficult, due to the nonselective feature of chemical or thermal reduction.¹¹ Normally, a further
2 tedious lithographic procedure is needed to accomplish the pattern formation.^{42,43} On the other hand, a
3 photoreduction strategy has the advantage to reduce GO in selected patterned areas only, when a
4 photomask is utilized.²⁴ Herein, we placed copper grids on the GO-PW films as photomasks and
5 realized a selected-area irradiation of UV-light. In this way, well-ordered conductive rGO rectangles in
6 micrometer size were directly patterned on the films. The optical images of the patterns are shown in
7 Figure 6A and 6B. Moreover, AFM images of the patterns in Figure S7 demonstrate that the reduced
8 and unreduced domains possess the same surface morphology. This suggests that the present UV-
9 photoreduction assisted patterning procedure, without any additional etching process, is mild and does
10 not affect the intrinsic structure of the films.
11
12
13
14
15
16
17
18
19
20
21
22
23

24 To demonstrate the application of the as-fabricated rGO patterns, we employed them as
25 microelectrodes for photodetector devices by spin coating a thin film of the blend of Poly(3-
26 hexylthiophene) (P3HT) and 1-(3-methoxycarbonyl)propyl-1-phenyl[6,6]C₆₁ (PCBM) on the patterns.
27 P3HT/PCBM blend is a classical active component for bulk-heterojunction solar cells, which shows a
28 strong photo-induced charge-separation performance.⁴⁴ Here, we used them as photoswitching material
29 in the photodetectors. The scheme of the photodetector is illustrated in Figure 6C. The detector is
30 typically composed of two adjacent rGO patterns as electrodes and the bridging P3HT/PCBM film
31 between them. The photoswitching property of the photodetector based on (PAH/GO/PAH/PW)₆ films
32 was investigated, which exhibited a well repeatable photocurrent response with an on/off ratio of ~ 3,
33 under the switching stimulus of external light source (see Figure 6D).
34
35
36
37
38
39
40
41
42
43
44
45
46

47 Conclusion

48 We have developed a facile and environmentally benign method for the fabrication of rGO composite
49 films, which combines LBL assembly and in-situ photoreduction procedures. In this method, GO
50 nanosheets and PW clusters are alternately deposited on substrates via electrostatic adsorption, followed
51 by an UV-photoreduction procedure converting GO to conductive rGO due to the photocatalytic role of
52 PW.²⁶ By this means, large-area, smooth and uniform rGO-PW composite films can be easily fabricated
53
54
55
56
57
58
59
60

1 on various substrates like quartz glass, silicon wafers and flexible polymers. We prepared FET devices
2 based on the composite films. The devices show ambipolar characteristics and tunable charge-carrier
3 mobilities which can be adjusted by controlling the number of deposited rGO layers. Furthermore, we
4 used photomasks to prepare photoreduced, conductive rGO patterns on the films and demonstrate their
5 function as microelectrodes for photodetectors. Taking into account the simple and efficient fabrication
6 procedure, this work offers a new strategy to prepare ultrathin rGO films with high quality and
7 uniformity, which facilitates application of the intriguing electronic properties of graphene. Moreover,
8 the performance of rGO devices prepared by our method can be further improved by using the large
9 sized GO nanosheets reported recently, which exhibit much higher electrical conductivities and carrier
10 mobilities.^{45,46} On the other hand, it can be envisioned that multifunctional rGO devices can be achieved
11 by incorporating different functional polyoxometalates: for example, the integration of magnetic
12 polyoxometalate clusters into rGO films can lead to new molecular memory devices;⁴⁷ besides, the
13 construction of logic-gate devices with dual optical and electrical output function will become possible
14 by a rational combination of the luminescent property of polyoxometalate clusters with the electric
15 response of rGO films.⁴⁸

16
17
18
19
20
21
22
23
24
25
26
27
28
29
30
31
32
33
34
35
36 **Acknowledgement.** This work was financially supported by Alexander von Humboldt Foundation to
37 H. Li, and the Max Planck Society through the program ENERCHEM, DFG MU 334/32-1, DFG
38 Priority Program SPP 1459, BMBF Project Graphenoid, BMBF Project LiBZ, ESF Project GOSPEL
39 (Ref Nr: 09-EuroGRAPHENE-FP-001), EU Project MOLESOL, EU Project GENIUS and ERC grant on
40 NANOGRAPH.. We thank G. Herrmann and W. Scholdei for considerable technical assistance and D.
41 Zheng from Jilin University for XPS measurements.

42
43
44
45
46
47
48
49
50
51 **Supporting Information Available.** Detailed experimental procedures; UV-vis absorption spectra of
52 the detailed LBL assembly process of a (PAH/GO/PAH/PW)₁ multilayer film (Figure S1); Plots of the
53 absorbance values of four separately prepared (PAH/GO/PAH/PW)_n multilayer films with n = 1–6 at
54 230, 260, 300 nm as a function of n (Figure S2, S3, and S4); SEM images of (PAH/GO/PAH/PW)₆ films
55
56
57
58
59
60

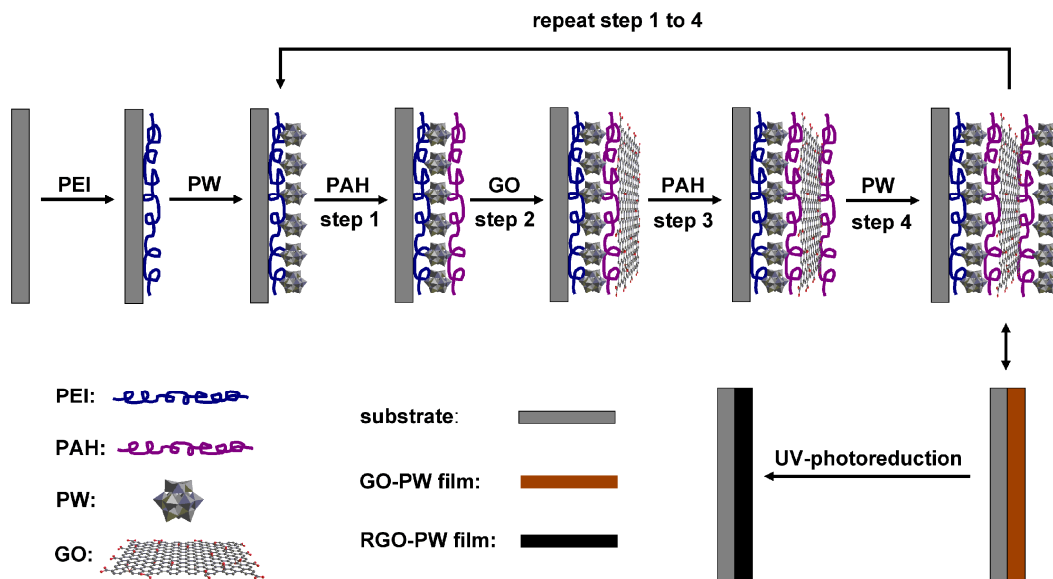
(Figure S5); AFM images and height profiles of the scarifications on (PAH/GO/PAH/PW)₁ and (PAH/GO/PAH/PW)₆ films (Figure S6); Detailed optical images and AFM images of the reduced patterns on a (PAH/GO/PAH/PW)₆ film (Figure S7). This information is available free of charge via the Internet at <http://pubs.acs.org>.

References

- [1] Novoselov, K. S.; Geim, A. K.; Morozov, S. W.; Jiang, D.; Zhang, Y.; Dubonos, S. W.; Grigorieva, I. V.; Firsov, A. A. *Science* **2004**, *306*, 666–669.
- [2] Geim, A. K.; Novoselov, K. S. *Nat. Mater.* **2007**, *6*, 183–191.
- [3] Geim, A. K. *Science* **2009**, *324*, 1530–1534.
- [4] Dreyer, D. R.; Ruoff, R. S.; Bielawski, C. W. *Angew. Chem. Int. Ed.* **2010**, *49*, 9336–9344.
- [5] Cai, J.; Ruffieux, P.; Jaafar, R.; Bieri, M.; Braun, T.; Blankenburg, S.; Muoth, M.; Seitsonen, A. P.; Saleh, M.; Feng, X. L.; Müllen, K.; Fasel, R. *Nature* **2010**, *466*, 470–473.
- [6] Schwierz, F. *Nat. Nanotechnol.* **2010**, *5*, 487–496.
- [7] Bonaccorso, F.; Sun, Z.; Hasan, T.; Ferrar, A. C. *Nat. Photon.* **2010**, *4*, 611–622.
- [8] Zhu, Y.; Murali, S.; Cai, W.; Li, X.; Suk, J. W.; Potts, J. R.; Ruoff, R. S. *Adv. Mater.* **2010**, *22*, 3906–3924.
- [9] Dreyer, D. R.; Park, S.; Bielawski, C. W.; Ruoff, R. S. *Chem. Soc. Rev.* **2010**, *39*, 228–240.
- [10] Park, S.; Ruoff, R. S. *Nat. Nanotechnol.* **2009**, *4*, 217–224.
- [11] Eda, G.; Chhowalla, M. *Adv. Mater.* **2010**, *22*, 2392–2415.
- [12] Gilje, S.; Han, S.; Wang, M.; Wang, K. L.; Kaner, R. B. *Nano. Lett.* **2007**, *7*, 3394–3398.
- [13] Wang, X.; Zhi, L.; Müllen, K. *Nano. Lett.* **2008**, *8*, 323–327.

- 1
2
3
4
5
6
7
8
9
10
11
12
13
14
15
16
17
18
19
20
21
22
23
24
25
26
27
28
29
30
31
32
33
34
35
36
37
38
39
40
41
42
43
44
45
46
47
48
49
50
51
52
53
54
55
56
57
58
59
60
- [14] Liang, Y. Y.; Zhi, L. J.; Norouzi-Arasi, H.; Feng, X. L.; Müllen, K. *Nanotechnology* **2009**, *20*, 434007.
- [15] Eda, G.; Fanchini, G.; Chhowalla, M. *Nat. Nanotechnol.* **2008**, *3*, 270–274.
- [16] Li, D.; Müller, M. B.; Gilje, S.; Kaner, R. B.; Wallace, G. G. *Nat. Nanotechnol.* **2008**, *3*, 101–105.
- [17] Decher, G. *Science* **1997**, *277*, 1232–1237.
- [18] Fendler, J. H. *Chem. Mater.* **1996**, *8*, 1616–1624.
- [19] Hammond, P. T. *Adv. Mater.* **2004**, *16*, 1271–1293.
- [20] Kotov, N. A.; Dékány, M.; Fendler, J. H. *Adv. Mater.* **1996**, *8*, 637–641.
- [21] Zhao, X.; Zhang, Q.; Hao, Y.; Li, Y.; Fang, Y.; Chen D. *Macromolecules* **2010**, *43*, 9411–9416.
- [22] Williams, G.; Seger, B.; Kamat, P. V. *ACS Nano* **2008**, *2*, 1487–1491.
- [23] Williams, G.; Kamat, P. K. *Langmuir* **2009**, *25*, 13869–13873.
- [24] Cote, L. J.; Cruz-Silva, R.; Huang, J. *J. Am. Chem. Soc.* **2009**, *131*, 11027–11032.
- [25] Manga, K. K.; Zhou, Y.; Yan, Y.; Loh, K. P. *Adv. Funct. Mater.* **2009**, *19*, 3638–3643.
- [26] Li, H.; Pang, S.; Feng, X.; Müllen, K.; Bubeck, C. *Chem. Commun.* **2010**, *46*, 6243–6245.
- [27] Caruso, F.; Kurth, D. G.; Volkmer, D.; Koop, M. J.; Müller, A. *Langmuir* **1998**, *14*, 3462–3465.
- [28] Moriguchi, I.; Fendler, J. H. *Chem. Mater.* **1998**, *10*, 2205–2211.
- [29] Ichinose, I.; Tagawa, H.; Mizuki, S.; Lvov, Y.; Kunitake, T. *Langmuir* **1998**, *14*, 187–192.
- [30] Kurth, D. G.; Volkmer, D.; Ruttorf, M.; Richter, B.; Müller, A. *Chem. Mater.* **2000**, *12*, 2829–2831.
- [31] Liu, S.; Kurth, D. G.; Bredenkötter, B.; Volkmer, D. *J. Am. Chem. Soc.* **2002**, *124*, 12279–12287.

- 1 [32] Hummers, W. S.; Offeman, R. E. *J. Am. Chem. Soc.* **1958**, *80*, 1339–1339.
- 2
- 3 [33] Vesel, A.; Mozetic, M.; Zalar, A. *Vacuum* **2008**, *82*, 248–251.
- 4
- 5
- 6 [34] Li, D.; Swanson, B. I.; Robinson, J. M.; Hoffbauer, M. A. *J. Am. Chem. Soc.* **1993**, *115*, 6975–6980.
- 7
- 8
- 9
- 10 [35] Keggin, J. F. *Proc. Roy. Soc. A* **1934**, *144*, 75–100.
- 11
- 12
- 13 [36] Hiskia, A.; Mylonas, A.; Papaconstantinou, E. *Chem. Soc. Rev.* **2001**, *30*, 62–69.
- 14
- 15
- 16 [37] Li, H.; Yang, Y.; Wang, Y.; Li, W.; Bi, L.; Wu, L. *Chem. Commun.* **2010**, *46*, 3750–3752.
- 17
- 18
- 19 [38] Stankovich, S.; Dikin, D. A.; Piner, R. D.; Kohlhaas, K. A.; Kleinhammes, A.; Jia, Y.; Wu, Y.;
- 20
21
22
23
24
25
26
27
28
29
30
31
32
33
34
35
36
37
38
39
40
41
42
43
44
45
46
47
48
49
50
51
52
53
54
55
56
57
58
59
60
- Nguyen, S. T.; Ruoff, R. S. *Carbon* **2007**, *45*, 1558–1565.
- [39] Eda, G.; Chhowalla, M. *Nano. Lett.* **2009**, *9*, 814–818.
- [40] Yamaguchi, H.; Eda, G.; Mattevi, C.; Kim, H.; Chhowalla, M. *ACS Nano* **2010**, *4*, 524–528.
- [41] Kobayashi, T.; Kimura, N.; Chi, J.; Hirata, S.; Hobarra, D. *Small* **2010**, *6*, 1210–1215.
- [42] Pang, S.; Tsao, H. N.; Feng, X.; Müllen, K. *Adv. Mater.* **2009**, *21*, 3488–3491.
- [43] Yao, P.; Chen, P.; Jiang, L.; Zhao, H.; Zhu, H.; Zhou, D.; Hu, W.; Han, B.; Liu, M. *Adv. Mater.* **2010**, *22*, 5008–5012.
- [44] Dennler, G.; Scharber, M. C.; Brabec, C. J. *Adv. Mater.* **2009**, *21*, 1323–1338.
- [45] Zhao, J.; Pei, S.; Ren, W.; Gao, L.; Chen, H. *ACS Nano* **2010**, *4*, 5245–5252.
- [46] Wang, S.; Ang, P. K.; Wang, Z.; Tang, A. L. L.; Tong, J. T. L.; Loh, K. P. *Nano. Lett.* **2010**, *10*, 92–98.
- [47] Lehmann, J.; Gaita-arino, A.; Coronad, E.; Loss, D. *Nat. Nanotechnol.* **2007**, *2*, 312–317.
- [48] Zhang, H.; Lin, X.; Yan, Y.; Wu, L. *Chem. Commun.* **2006**, 4575–4577.



Scheme 1. Schematic illustration of the fabrication procedure of rGO-PW multilayer films, which involves the LBL assembly of GO nanosheets and PW clusters using cationic polyelectrolytes PEI and PAH as electrostatic linkers, and a subsequent in-situ photoreduction to convert GO to rGO.

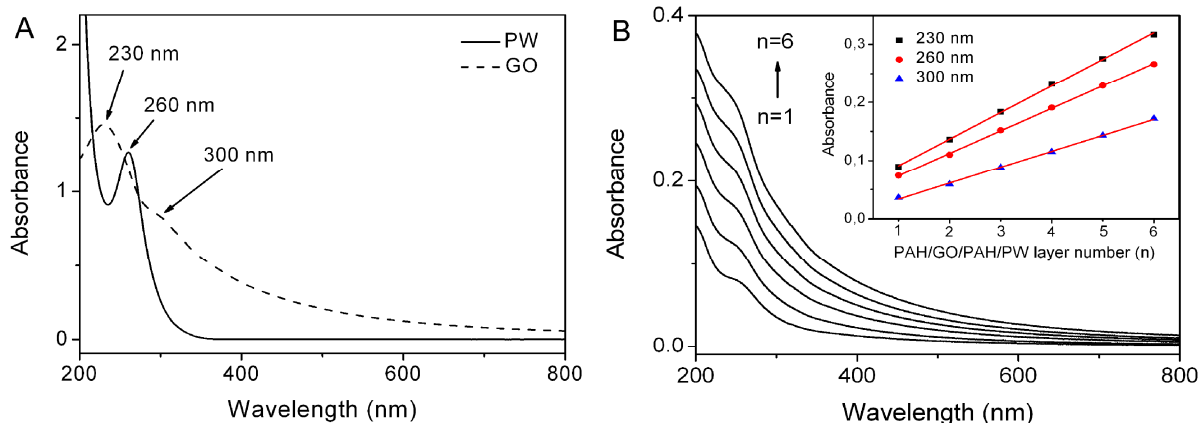


Figure 1. Part A shows the UV-Vis absorption spectra of an aqueous 0.05 mg/mL PW solution (black line, PW concentration is 1.7×10^{-5} M) and an aqueous 0.05 mg/mL GO solution (red line); Part B presents the UV-Vis absorption spectra of LBL-assembled (PAH/GO/PAH/PW)_n multilayer films with layer number n = 1–6 on a quartz substrate, which was modified before by a PEI/PW precursor film. The blank substrate was used as reference. The curves, from bottom to top, correspond to n = 1–6. Inset shows the plots of the absorbance values at 230, 260, 300 nm as a function of the layer number n.

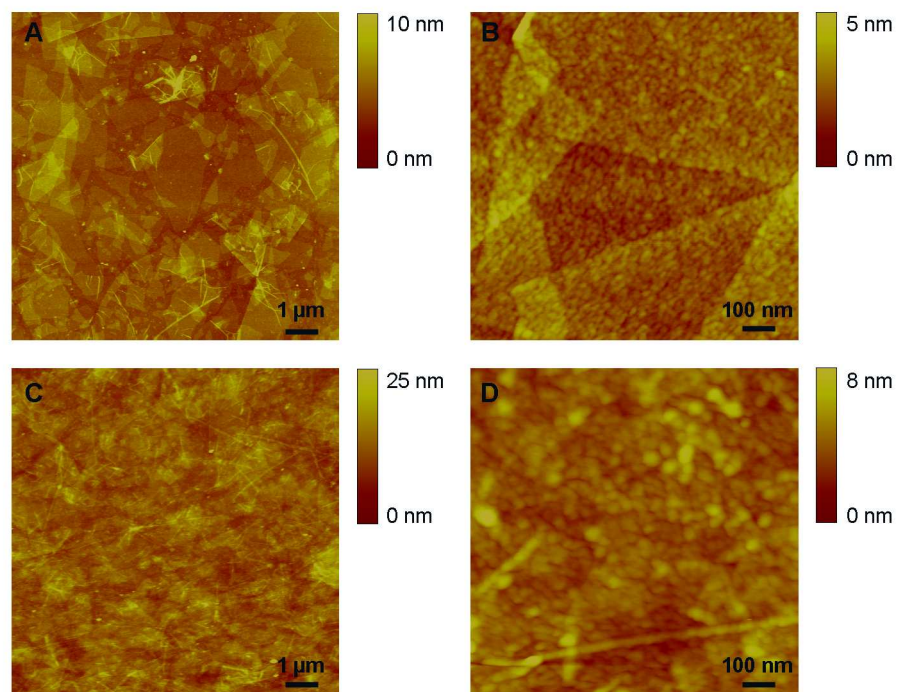


Figure 2. AFM images of a (PAH/GO/PAH/PW)₁ film (A and B) a (PAH/GO/PAH/PW)₆ film (C and D) both on PEI/PW precursor film modified silicon substrates, which contain 300 nm thermal oxide.

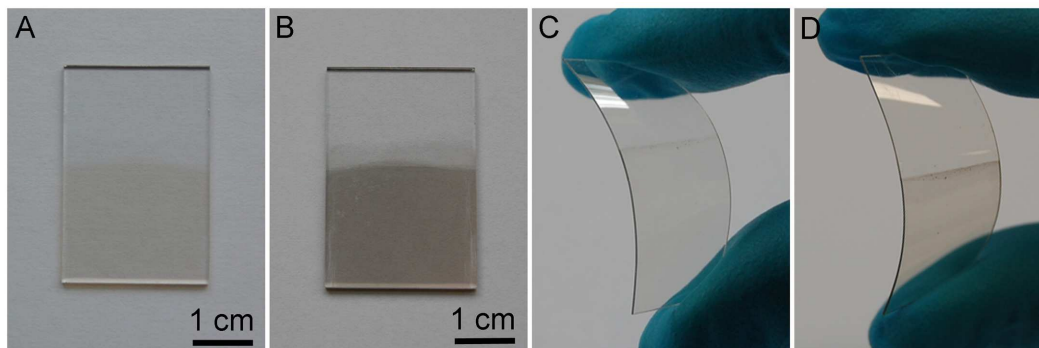


Figure 3. Optical images of a (PAH/GO/PAH/PW)₆ multilayer film prepared on a quartz substrate before (A) and after (B) 6 hour UV-photoreduction, and on a flexible PET substrate before (C) and after (D) 6 hour UV-photoreduction. Both substrates are coated first by a PET/PW precursor film.

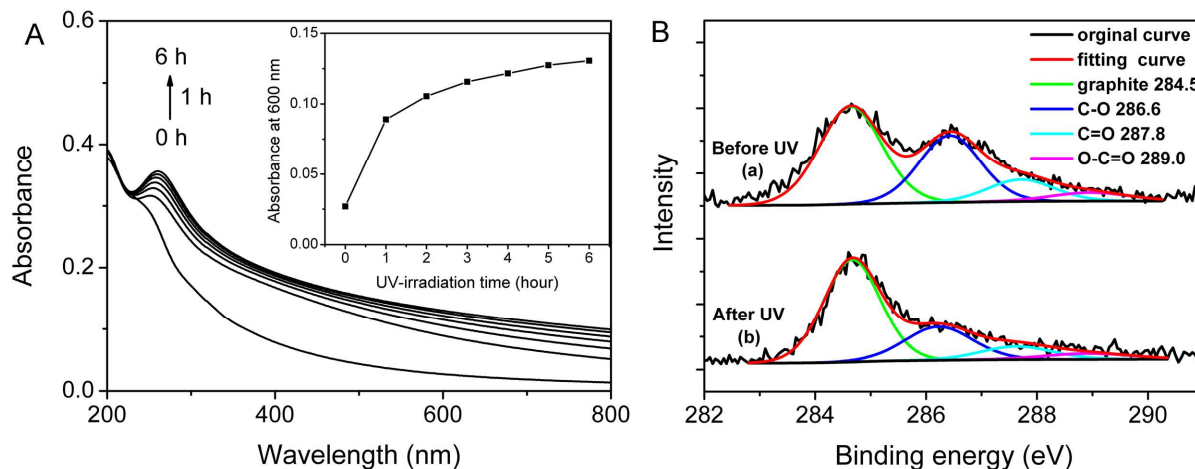


Figure 4. Part A shows the UV-Vis spectra of a (PAH/GO/PAH/PW)₆ multilayer film prepared on a PEI/PW precursor film modified quartz substrate after various irradiation times of the UV-photoreduction process. The inset shows absorbance values at 600 nm as a function of the irradiation time. Part B shows the C 1s XPS spectra of a (PAH/GO/PAH/PW)₆ film on a PEI/PW precursor film modified quartz substrate before (curve a) and after (curve b) 6 hour UV-photoreduction.

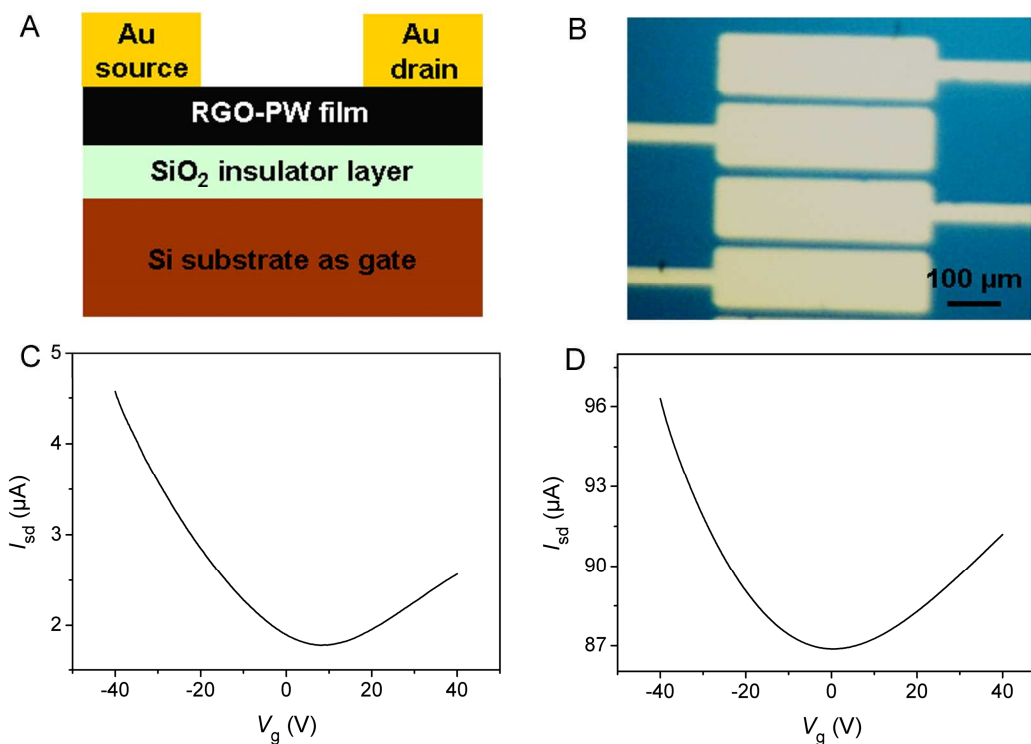


Figure 5. Part A illustrates the rGO-PW film based FET devices (cross section); Part B is the optical microscope image of the actual device (top view). The blue part is the surface of the rGO-PW films. The Au electrodes appear bright. Parts C and D display the I_{ds} - V_g curves of the FET devices fabricated on a (PAH/GO/PAH/PW)₁ film and a (PAH/GO/PAH/PW)₆ film, respectively. Both samples are prepared on PEI/PW precursor film modified silicon substrates with 300 nm thermal oxide and have undergone 6 hours UV-photoreduction. V_{sd} is 10 V.

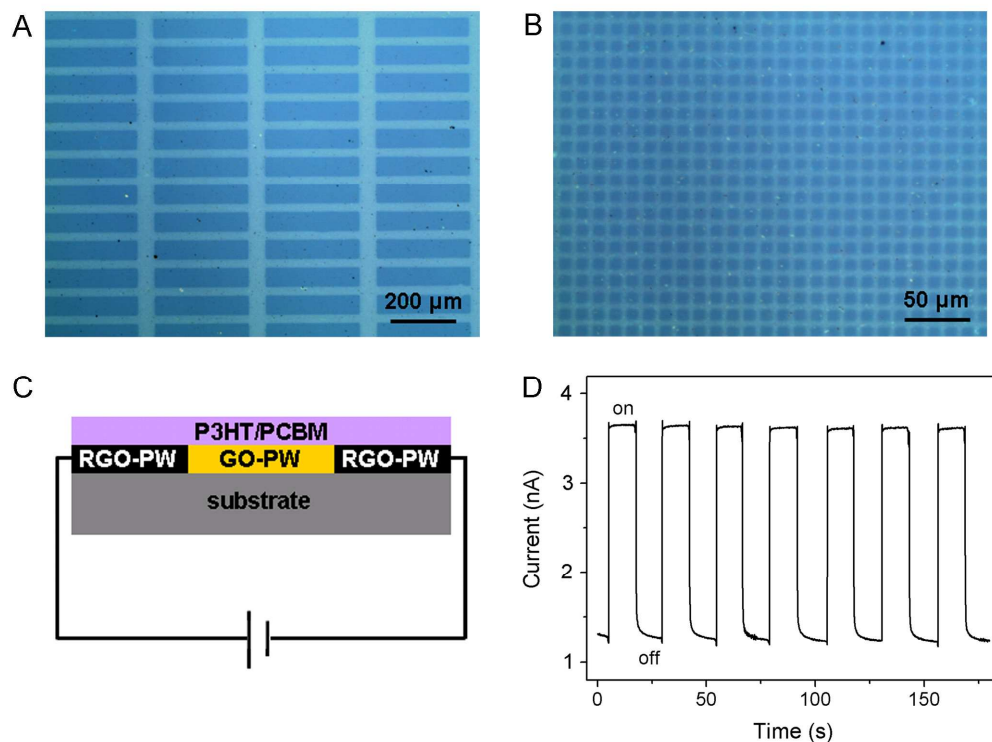


Figure 6. Optical microscope images of reduced patterns on $(\text{PAH}/\text{GO}/\text{PAH}/\text{PW})_6$ multilayer films on PEI/PW precursor film modified silicon substrates with 300 nm thermal oxide (A and B). The patterns are made by 6 hour UV-photoreduction using different photomasks. Part C illustrates the cross-section of the photodetector device using conductive patterns of rGO-PW film as microelectrodes and the photo-switching material P3HT/PCBM, which is spin coated on the patterns; Part D shows the photocurrent response of the photodetector based on the conductive patterns in part A versus time under chopped irradiation, at a bias voltage of 10 V.

Table 1. Fitting results of the C 1s XPS spectra shown in Figure 4B of the (PAH/GO/PAH/PW)₆ film before and after 6 hour UV-photoreduction.

Type of carbon	Binding energy (eV)	Before photoreduction (relative area %)	After photoreduction (relative area %)
graphite	284.5	44.8	65.6
C-O	286.6	41.1	20.9
C=O	287.8	9.9	9.7
O-C=O	289.0	4.2	3.8

1
2
3
4 **Table of contents:**
5
6

7 Haolong Li, Shuping Pang, Si Wu, Xinliang Feng,* Klaus Müllen,* Christoph Bubeck*
8
9

10 Layer-by-layer assembly and UV-photoreduction of graphene-polyoxometalate composite films for
11 electronics
12
13
14
15
16
17
18
19

